Theor Chem Acc (2011) 130:37–50
DOI 10.1007/s00214-011-0956-2

REGULAR ARTICLE

Theoretical investigation of one- and two-photon spectra of pyrazabole chromophores

Xiao-Ting Liu · Lu-Yi Zou · Ai-Min Ren · Jing-Fu Guo · Ying Sun · Shuang Huang · Ji-Kang Feng

Received: 21 January 2011 / Accepted: 3 May 2011 / Published online: 15 May 2011

Abstract An extensive series of pyrazabole chromophores containing pseudo-conjugated systems have been theoretically constructed and investigated on the one-photon absorption (OPA) and two-photon absorption (TPA) properties by using density functional theory and Zerner's intermediate neglect of differential overlap methods. The results indicated that all the pyrazabole chromophores show strong OPA at around 400 nm and intense TPA properties in the range of 500–600 nm with TPA cross sections (δ_{max}) as large as 540–3,560 GM, which are excellent candidates for optical power limiting materials. It is noteworthy that the δ_{max} values of the two constructed pyrazaboles, **PA3** and **PAF2,** are 308.8 GM at 772.0 nm and 157.8 GM at 834.4 nm, respectively, which may be particularly attractive as probes for two-photon fluorescence imaging. The influence of incorporating electron acceptors in the central core, π-conjugated bridge and terminal groups on OPA and TPA properties was analyzed in detail to derive structure–property relationships and to lay the guidelines for both spectral tuning and amplification of molecular TPA in the target region. Meanwhile, the solvent effects on these properties were taken into account within the PCM model. The solvent has a significant impact on the TPA properties for chromophore **PA3** and leads to the two-photon absorption spectra (λ^T_{max}) red-shift and δ_{max} enhancing relative to those in gas phase. In addition, from the calculations of molecule **AlA2**, we can draw the conclusion that the compounds with the Al_2N_4 center behave similarly to pyrazabole chromophores in the linear optical and TPA properties and increase TPA cross sections to some extent.

Keywords Pyrazabole chromophores · Two-photon absorption · Electronic structure · Density functional theory · Non-linear optical property

1 Introduction

Nowadays, there is a strong demand for efficient two-photon absorption (TPA) materials as a result of a wide range of applications, including microscopy [1], microfabrications [2], three-dimensional data-storage [3], optical power limiting [4], photodynamic therapy [5], up-converted lasing [6], and two-photon excited fluorescence (TPEF) microscopy of biological systems [7]. This demand has been matched by rapid advances in the design and synthesis of TPA dyes with large TPA cross sections (δ_{max}) [8]. The construction of molecules with large δ_{max} has been investigated both experimentally [9–12] and theoretically [13–17]. In particular, most explored and efficient TPA dyes have a symmetric rigid rod structure and can be described as a couple of electron-donating (D) and/or electron-accepting (A) in interaction through a conjugated central core [18]. On the basis of this general setting, many factors play a dominant role in enhancing TPA cross

Electronic supplementary material The online version of this article (doi:10.1007/s00214-011-0956-2) contains supplementary material, which is available to authorized users.

X.-T. Liu · L.-Y. Zou · A.-M. Ren (✉) · Y. Sun · S. Huang · J.-K. Feng
State Key Laboratory of Theoretical and Computational Chemistry, Institute of Theoretical Chemistry, Jilin University, Changchun 130023, People's Republic of China
e-mail: aimin_ren@yahoo.com

J.-F. Guo
School of Physics, Northeast Normal University, Changchun 130021, People's Republic of China

sections, such as the conjugation length, the molecular planarity, the electronic coupling, the electron-donating and electron-accepting strength of the substituents, and the dimensionality of the charge-transfer network.

Although a great variety of efficient TPA chromophores are already available, many of them consist only from substituted conjugated aromatic rings and depend on the optical properties of simple electron-donating and/or electron-accepting functionalities. Replacement of these rigid aromatic systems with π-excessive or π-deficient heteroaromatics has been shown to result in an increased intramolecular charge transfer (ICT), as well as enhanced two-photon absorption [19–23]. Moreover, boron-containing heterocyles that behave as a pseudo-conjugated system have been recently used for fine-tuning of the electronic and optical properties [24, 25].

It is reported that organoboron dyes exhibit various interesting properties due to the high electron affinity of boron atoms, such as large molar extinction coefficients, two-photon absorption cross sections, high emission quantum yields, and sensitivity to the surrounding medium [26]. Because of their unique properties, they have been expected as a novel type of optical and electronic materials in the past decade [27].

Pyrazabole is known as a highly stable boron heterocycle in which a variety of functional groups can be readily introduced. And some applications of these pyrazaboles have been performed in the past decades such as liquid crystals [28–30], π-conjugated hybrid polymers [27, 31]. Moreover, some investigations reported that the pyrazabole moiety, another boron-containing pseudo-conjugated system, could be interesting for obtaining new luminescent materials [25, 32]. In 2009, Nicoud et al. prepared some pyrazabole fluorophores and characterized their one and two-photon photophysical properties. And the experimental results indicated that these fluorophores exhibited high TPA cross sections, efficient fluorescence in organic solvents and can be used in two-photon excited microscopy images [25]. Furthermore, the boat conformation of the pyrazabole ring is of particular interest in the preparation of new bent polar materials as the molecules in the boat conformation exhibits a dipole moment in the bent direction [33]. This may be important for affecting the nonlinear optical (NLO) properties including TPA properties. Thereby it is necessary to study the relationship between structural and NLO properties in this kind of compounds.

However, to the best of our knowledge, the linear optical and TPA properties of pyrazabole chromophores have not been investigated theoretically up to date. Within this context, we designed some pyrazaboles containing nitryl, benzothiazole, and other functionalities and performed density functional theory (DFT) and Zerner's intermediate neglect of differential overlap (ZINDO) methods to investigate the linear optical absorption, as well as TPA properties. Our aim was to understand the influence of this unusual structure on the efficiency of NLO properties due to electronic coupling through such a pseudo-conjugated system. We believe that this detailed computational study performed on an extensive series of pyrazaboles will contribute to the overall understanding of structure-properties relationships of TPA chromophores.

2 Computational details

In this study, the ground-state geometries of all molecules were fully optimized without any symmetric constraints by using DFT with the 6-31G(d) basis set and the hybrid three-parameter Becke exchange functional and Lee-Yang Parr correction functional (B3LYP). Frequency calculations were carried out to verify the identity of each stationary point as a minimum. All calculations were performed by using Gaussian 03 and Gaussian 09 program packages [34, 35]. On the basis of the optimized structures, the OPA properties of the studied molecules were calculated by employing the ZINDO program including single and double electronic excitation configuration interactions. The absorption spectra were also investigated by the time-dependent density functional theory (TDDFT) at the same level. In addition, the solvent effects were taken into account by means of the polarized continuum model (PCM) approach [36–38].

The TPA process corresponds to simultaneous absorption of two photons. The TPA efficiency of an organic molecule, at optical frequency $\omega/2\pi$, can be characterized by the TPA cross section $\delta(\omega)$. It can be directly related to the imaginary part of the third-order polarizability γ $(-\omega;$ $\omega, -\omega, \omega)$ by [39, 40]:

$$\delta(\omega) = \frac{3\hbar\omega^2}{2n^2c^2\varepsilon_0} L^4 \mathrm{Im}[\gamma(-\omega;\omega,-\omega,\omega)] \quad (1)$$

in which γ $(-\omega;$ $\omega,$ $\omega,$ $\omega)$ is the third-order polarizability, $\hbar\omega$ is the energy of incoming photons, c is the speed of light, ε_0 is the vacuum electric permittivity, n denotes the refractive index of medium, and L corresponds to the local-field factor. In the calculations presented here, n and L are set to 1 because of isolated molecule in vacuum.

The components of the third-order polarizability $\gamma_{\alpha\beta\gamma\delta}$ can be evaluated by a sum-over-states (SOS) expression. By considering a Taylor expansion of energy with respect to the applied field, the Cartesian components $\gamma_{\alpha\beta\gamma\delta}$ are given by [41, 42]:

$$\gamma_{\alpha\beta\gamma\delta}(-\omega_\sigma;\,\omega_1,\,\omega_2,\,\omega_3)=\hbar^{-3}\sum P_{1,2,3}\Bigg(\sum_K{}'\sum_L{}'\sum_M{}'\times\Bigg(\frac{\langle 0|\mu_\alpha|K\rangle\langle K|\overline{\mu_\beta}|L\rangle\langle L|\overline{\mu_\gamma}|M\rangle\langle M|\mu_\delta|0\rangle}{(\omega_K-i\Gamma_K-\omega_\sigma)(\omega_L-i\Gamma_L-\omega_2-\omega_3)(\omega_M-i\Gamma_M-\omega_3)}+\frac{\langle 0|\mu_\beta|K\rangle\langle K|\overline{\mu_\alpha}|L\rangle\langle L|\overline{\mu_\gamma}|M\rangle\langle M|\mu_\delta|0\rangle}{(\omega_K+i\Gamma_K+\omega_1)(\omega_L-i\Gamma_L-\omega_2-\omega_3)(\omega_M-i\Gamma_M-\omega_3)}+\frac{\langle 0|\mu_\beta|K\rangle\langle K|\overline{\mu_\gamma}|L\rangle\langle L|\overline{\mu_\alpha}|M\rangle\langle M|\mu_\delta|0\rangle}{(\omega_K+i\Gamma_K+\omega_1)(\omega_L+i\Gamma_L+\omega_1+\omega_2)(\omega_M-i\Gamma_M-\omega_3)}+\frac{\langle 0|\mu_\beta|K\rangle\langle K|\overline{\mu_\gamma}|L\rangle\langle L|\overline{\mu_\delta}|M\rangle\langle M|\mu_\alpha|0\rangle}{(\omega_K+i\Gamma_K+\omega_1)(\omega_L+i\Gamma_L+\omega_1+\omega_2)(\omega_M+i\Gamma_M+\omega_\sigma)}\Bigg)-\sum_K{}'\sum_L{}'\Bigg(\frac{\langle 0|\mu_\alpha|K\rangle\langle K|\mu_\beta|0\rangle\langle 0|\mu_\gamma|L\rangle\langle L|\mu_\delta|0\rangle}{(\omega_K-i\Gamma_K-\omega_\sigma)(\omega_K-i\Gamma_K-\omega_1)(\omega_L-i\Gamma_L-\omega_3)}+\frac{\langle 0|\mu_\alpha|K\rangle\langle K|\mu_\beta|0\rangle\langle 0|\mu_\gamma|L\rangle\langle L|\mu_\delta|0\rangle}{(\omega_K-i\Gamma_K-\omega_1)(\omega_L+i\Gamma_L+\omega_2)(\omega_L-i\Gamma_L-\omega_3)}+\frac{\langle 0|\mu_\beta|K\rangle\langle K|\mu_\alpha|0\rangle\langle 0|\mu_\gamma|L\rangle\langle L|\mu_\delta|0\rangle}{(\omega_K+i\Gamma_K+\omega_1)(\omega_K+i\Gamma_K+\omega_\sigma)(\omega_L+i\Gamma_L+\omega_2)}+\frac{\langle 0|\mu_\beta|K\rangle\langle K|\mu_\alpha|0\rangle\langle 0|\mu_\gamma|L\rangle\langle L|\mu_\delta|0\rangle}{(\omega_K+i\Gamma_K+\omega_1)(\omega_L+i\Gamma_L+\omega_2)(\omega_L-i\Gamma_L-\omega_3)}\Bigg)\Bigg)\tag{2}$$

In this formula, α, β, γ, and δ refer to the molecular axes; and ω_1, ω_2, and ω_3 are incident optical frequencies; and $\omega_\sigma=\omega_1+\omega_2+\omega_3$ is the polarization response frequency; $\sum P_{1,2,3}$ indicates a sum over the terms obtained by the six permutations of the pairs (ω_1/μ_β), (ω_2/μ_γ), and (ω_3/μ_δ); K, L, and M denote excited states, and 0 denotes the ground state; $|K\rangle$ is an electronic wave function with energy $\hbar\omega_K$ relative to the ground electronic state; μ_α is the αth (=x, y, z) component of the dipole operator, $\langle K|\overline{\mu_\alpha}|L\rangle=\langle K|\mu_\alpha|L\rangle-\langle 0|\mu_\alpha|0\rangle$; the primes on the summation over the electronic states indicate exclusion of the ground state. And Γ_K is the damping factor of excited state K and in the present work all damping factors are set to 0.1 eV [43, 44].

To compare the calculated δ value with the experimental value measured in solution, the orientationally averaged (isotropic) value of γ is evaluated, which is defined as

$$\langle\gamma\rangle=\frac{1}{15}\sum_{i,j}\left(\gamma_{iijj}+\gamma_{ijij}+\gamma_{ijji}\right)\quad i,j=x,\,y,\,z\tag{3}$$

Taking the imaginary part of $\langle\gamma\rangle$ value into the expression (1), $\delta(\omega)$ can be obtained as compared to the experimental data.

In principle, any kind of self-consistent-field molecular orbital procedure combined with the configuration interaction (CI) can be used to calculate the physical values in the above expression. In this work, the properties of electronic excited states were obtained by single and double electronic excitation configuration interaction using the ZINDO program. For all the molecules, the CI-active spaces were restricted to the 39 highest-occupied and 39 lowest-unoccupied π orbitals for the singly excited configuration, and to the 5 highest-occupied and 5 lowest-unoccupied π orbitals for the doubly excited configuration. Moreover, the transition energies and transition moments were also obtained by ZINDO calculations. Then, the FTRNLO program compiled by our group was used to calculate the second hyperpolarizability and TPA cross sections according to Eqs. (1–3). The calculated TPA cross sections of all fluorophores include the contributions from 300 lowest-lying excited states. The chosen number of 300 states was sufficient for the convergence of $\delta(\omega)$ in this paper, which was concluded from the relationship between $\delta(\omega)$ and the number of states for all the studied molecules.

3 Results and discussions

3.1 Molecular design and geometry optimization

The studied molecular structures are presented in Fig. 1. We performed the calculations on a series of model compounds (**P1**, **PA1**, **P2**, **PA2,** and **PAB**) for compounds **8**, **10**, **9**, **11,** and **13** in refer [25] where the long-chain alkyl groups that bond to boron atoms or terminal phenyl groups were all replaced by methyl groups. This kind of simplification has been successfully applied in the previous works [23, 44]. Fluorophores **PA1, PA2,** and **PE2** bearing electron-donating trialkoxyphenyl or diphenylamino terminal groups, were elongated π-systems by adding acetylene or ethylene as compared with **P1** or **P2**. And chromophore **PAB** contains electron-donating boron-dipyrromethene (BODIPY) group. Pyrazabole derivatives **PA3**, **PA4**, **PAN2**, **PAF2,** and **BA2** were constructed to study the effects of the introducing electron-acceptor in the central core, π-conjugated bridge, and terminal groups on OPA and TPA properties. The geometric structures were fully optimized with no symmetry constraint using the Gaussian 03 program with 6-31G* basis set at the B3LYP level. For the sake of confirming the stability of the optimized structures, the harmonic vibrational frequencies upon the optimized structures were evaluated at the same level, and the results show no imaginary frequency. The optimized ground-state geometries of some pyrazaboles and their energies (a.u.) are described in Fig. 2. As shown, all pyrazaboles studied have the stable conformation with the boat form. The boron atom has a distorted tetrahedral coordination in the bent structures, with the C–B–C (F–B–F) angles larger than the N–B–N angles. The bent angle between the mean planes of the two pyrazole rings is around 146° except molecule **BA2** (136°). Therefore, the compound with BF_2 group exhibits a more obvious bent shape than the ones with B $(CH_3)_2$ group. However, single-crystal X-ray analysis of several pyrazaboles shows that the

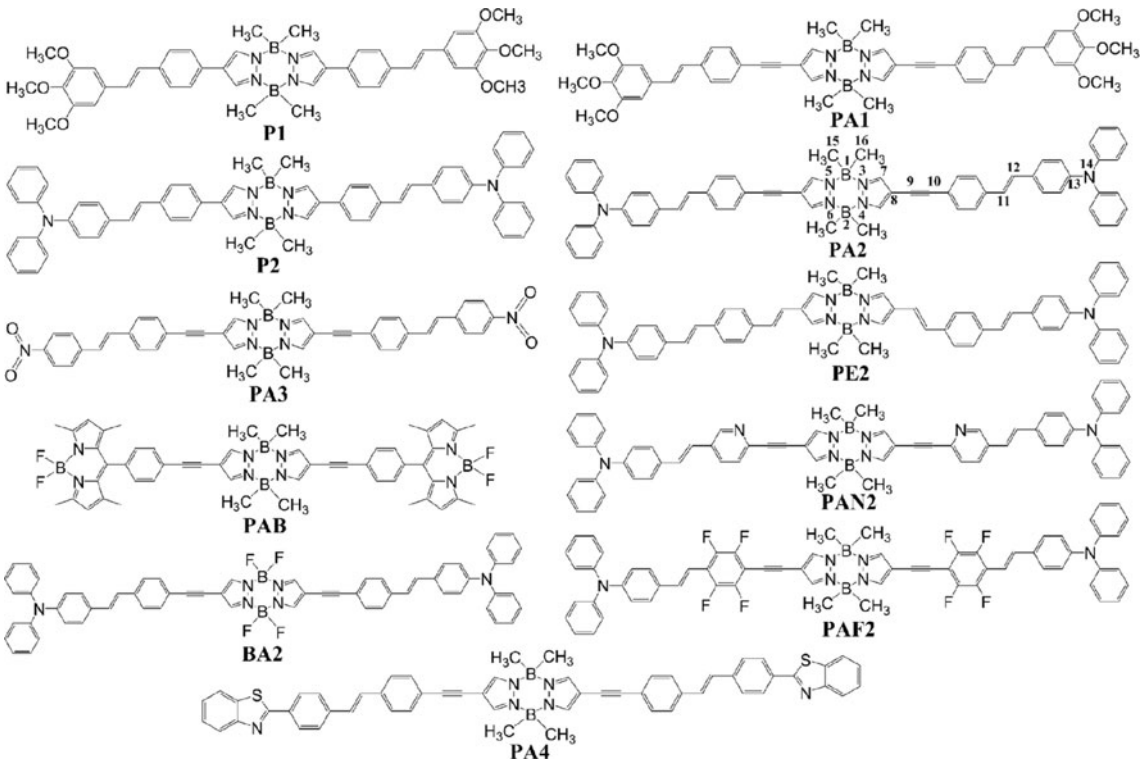

Fig. 1 Molecular structures of all the chromophores studied

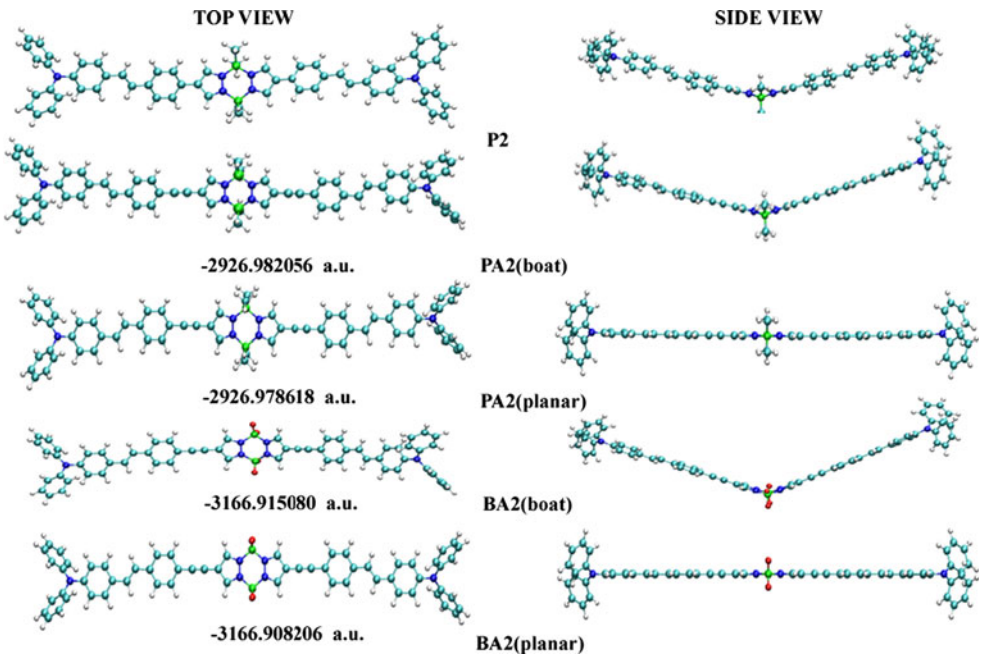

Fig. 2 The optimized ground-state geometries and energies of fluorophores **P2**, **PA2,** and **BA2**

central B_2N_4 ring can adopt a chair, flat, or boat conformation according to the functional groups at the boron atoms [33, 45, 46]. Thus, the planar and chair conformations of fluorophores **PA2** and **PE2** were performed on the optimization and frequency calculations. Interestingly, their starting chair conformation yields the final boat conformation. From analysis of the energy and frequency results, we can conclude that all the molecules adopt a bent shape as a result of the boat conformation of the central B_2N_4 ring. Furthermore, the inclusion solvent that may have some effect on the conformations was considered. Taking molecule **PA2** as an example, it was optimized by

performing DFT/PCM//B3LYP/6-31G* in dichloromethane. And the result demonstrates that it does yet display the boat conformation. Some important parameters of the optimized geometries with the stable conformation in the gas phase and dichloromethane are collected in Table S1. It is noteworthy that there are hardly any differences in these parameters, which implies that the influence of the solvent on the molecular geometry can be ignored in the computational process.

3.2 Electronic structures

The energies of some frontier orbitals [four occupied orbitals, four unoccupied orbitals and energy gaps between the highest occupied molecular orbital (HOMO), and the lowest unoccupied molecular orbital (LUMO)] obtained by B3LYP/6-31G* are shown schematically in Fig. 3. The energy of LUMO decreases with the π-conjugation length increasing, that is, **P1** (−1.52 eV) > **PA1** (−1.66 eV), and **P2** (−1.50 eV) > **PA2** (−1.68 eV) > **PE2** (−1.70 eV). However, the energy of HOMO is little influenced by the extension of conjugation length. Consequently, the energy gap between HOMO and LUMO (ΔE_{H-L}) decreases with the increase of the conjugated system length [3.68 eV (**P1**) > 3.51 eV (**PA1**) and 3.33 eV (**P2**) > 3.16 eV (**PA2**) > 3.08 eV (**PE2**)]. As the strength of the donors or acceptors in the terminal group increases, ΔE_{H-L} decreases: such as **P1** (3.68 eV) > **P2** (3.33 eV), **PA1** (3.51 eV) > **PA2** (3.16 eV) > **PAB** (2.99 eV), and **PA4** (3.24 eV) > **PA3** (3.11 eV). Comparing molecules **PA2** and its analogs **PAN2** and **PAF2**, in which spacers are modified by incorporating electron-withdrawing groups, one can find that the energies of HOMO and LUMO decrease, but the order of ΔE_{H-L} is **PA2** > **PAN2** > **PAF2**. Replacement of methyl with fluorine groups at the boron atoms makes ΔE_{H-L} of **BA2** smaller than that of **PA2**.

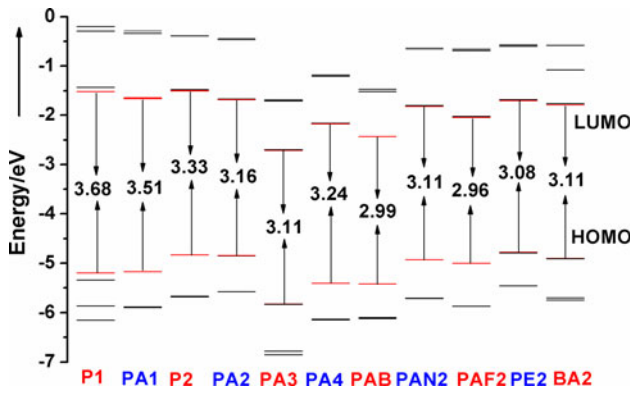

Fig. 3 Frontier orbital energies of fluorophores optimized at the B3LYP/6-31G(d) level

Interestingly, as can be seen from Fig. 3, the HOMO and HOMO-1 are almost degenerate in energy and well separated from the other orbitals; a similar trend is made for the LUMO and LUMO+1. In addition, to further investigate the above results, the frontier molecular orbitals (FMO) are displayed in Figure S1 (see Supporting Information). Impressively, the two highest HOMOs and two lowest LUMOs exhibit almost the same shapes due to their quasi-degeneracy and differ only from lobes symmetry considerations.

3.3 One-photon absorption properties

The OPA properties of all chromophores were calculated by means of the ZINDO program on the basis of the optimized geometric structures. In addition, TD-DFT//B3LYP/6-31G* method was also utilized to calculate the OPA properties for the sake of comparison. The corresponding data are collected in Table 1. As compared with the experimental results, the maximum values of UV/Vis absorption (λ_{max}^{O}) calculated by the B3LYP method are red-shifted by 10–50 nm, especially 100 nm for fluorophore **PAB**. When the solvent effect was considered, the calculated results in dichloromethane are bathochromically shifted by 10–20 nm relative those in gas and still deviate from the experimental data. B3LYP is not a perfect functional for this system, but when other basis sets and functionals in TD-DFT were used for calculating by testing compounds **PA2** and **PAB** and the results were worse (see Table S2 in the Supporting Information). However, the λ_{max}^{O} values of compounds **P1**, **PA1**, **P2**, **PA2,** and **PAB** obtained by ZINDO/SDCI (340.4, 379.9, 373.0, 389.6, and 474.2 nm) are in good agreement with the experimental data (343, 355, 379, 387, and 502 nm) [25]. This good result makes us confident that the computed spectra of the fluorophores not yet investigated experimentally should be reliable. Therefore, the ZINDO results will be used in the following discussion.

As clearly shown in Table 1, all fluorophores exhibit an intense absorption in the near UV/Vis blue region. Their absorption range can be tuned by changing the nature of the terminal groups, of the substitution at the boron atoms of the pyrazabole center, and the length of the π-conjugated systems. Substitution of the methyl with fluorine at the boron atoms produces a small red-shift of the absorption band, that is, **PA2** (389.6 nm) < **BA2** (392.0 nm). Increasing the conjugated length induces a significant bathochromic shift of the absorption band, which is just corresponding to the ΔE_{H-L} above. For example, the λ_{max}^{O} of **PA1** is red-shifted by 39.5 nm relative to **P1**. Changing the nature of the conjugated linker allows spectral tuning of the absorption characteristic. The replacement of a triple bond by a double bond does not

Table 1 One-photon absorption properties, λ_{max}^{O} (nm)

Mol.	ZINDO			TDDFT	
	λ_{max}^{O}	f	Transition nature	λ_{max}^{O}	f
P1	340.4 (343[a])	2.13	$S_0 \rightarrow S_1$ (H) $\rightarrow$ (L + 1)39% (H−1) $\rightarrow$ (L)30%	354.8	2.21
	339.1[b]	2.73[b]		361.8[b]	3.08[b]
PA1	379.9 (355[a])	2.24	$S_0 \rightarrow S_3$ (H − 1) $\rightarrow$ (L)28% (H) $\rightarrow$ (L + 1)28%	383.0	3.95
	376.9[b]	2.20[b]		391.6[b]	4.07[b]
P2	373.0 (379[a])	2.75	$S_0 \rightarrow S_1$ (H − 1) $\rightarrow$ (L)30% (H) $\rightarrow$ (L)22%	415.6	2.89
	376.4[b]	2.82[b]	(H) $\rightarrow$ (L + 1)19%	425.1[b]	3.00[b]
	311.1	0.43	$S_0 \rightarrow S_{14}$ (H) $\rightarrow$ (L + 9)20% (H − 1) $\rightarrow$ (L + 9)16%	323.4	1.14
	315.5[b]	0.28[b]	(H) $\rightarrow$ (L + 7)14% (H − 1) $\rightarrow$ (L + 7)11%	326.2[b]	0.87[b]
PA2	389.6 (387[a])	2.98	$S_0 \rightarrow S_1$ (H − 1) $\rightarrow$ (L + 1)29% (H) $\rightarrow$ (L)17%	436.9	3.44
	390.2[b]	2.88[b]	(H) $\rightarrow$ (L + 1)11%	453.7[b]	3.43[b]
	313.5	0.36	$S_0 \rightarrow S_{19}$ (H − 1) $\rightarrow$ (L + 8)29% (H − 1) $\rightarrow$ (L + 7)18%	346.1	1.34
	314.2[b]	0.28[b]		349.5[b]	1.50[b]
PA3	394.7	2.43	$S_0 \rightarrow S_5$ (H) $\rightarrow$ (L)16% (H − 1) $\rightarrow$ (L + 1)16%	432.8	2.73
	430.2[b]	2.03[b]	(H) $\rightarrow$ (L + 1)10% (H − 1) $\rightarrow$ (L)10%	462.5[b]	2.61[b]
	297.8	0.24	$S_0 \rightarrow S_{19}$ (H − 1) $\rightarrow$ (L + 3)18% (H) $\rightarrow$ (L + 3)14%	329.3	1.57
	367.9[b]	0.40[b]		341.0[b]	1.59[b]
PA4	400.6	3.75	$S_0 \rightarrow S_1$ (H − 1) $\rightarrow$ (L + 1)21% (H) $\rightarrow$ (L)20%	422.6	4.92
	396.2[b]	3.71[b]	(H) $\rightarrow$ (L + 1)15% (H − 1) $\rightarrow$ (L)15%	434.1[b]	4.99[b]
	314.1	0.19	$S_0 \rightarrow S_{16}$ (H) $\rightarrow$ (L + 3)20% (H − 1) $\rightarrow$ (L + 2)18%	341.4	0.11
	300.7[b]	0.21[b]	(H − 2) $\rightarrow$ (L + 2)13% (H − 3) $\rightarrow$ (L + 2)12%	342.1[b]	0.16[b]
PAB	474.2 (502[a])	1.03	$S_0 \rightarrow S_3$ (H − 1) $\rightarrow$ (L)29% (H) $\rightarrow$ (L + 1)28%	409.2	0.85
	454.6[b]	1.04[b]	(H − 1) $\rightarrow$ (L + 1)19% (H) $\rightarrow$ (L)19%	419.4[b]	1.01[b]
	350.4	0.93	$S_0 \rightarrow S_8$ (H − 2) $\rightarrow$ (L + 5)28% (H − 3) $\rightarrow$ (L + 4)28%	361.6	0.16
	341.6[b]	0.77[b]		361.2[b]	0.14[b]
PAN2	396.1	2.88	$S_0 \rightarrow S_1$ (H) $\rightarrow$ (L + 1)29% (H − 1) $\rightarrow$ (L)27%	444.1	3.27
	313.8	0.26	$S_0 \rightarrow S_{18}$ (H − 2) $\rightarrow$ (L + 3)18% (H − 3) $\rightarrow$ (L + 2)16%	346.9	1.50
	400.4[b]	2.46[b]	(H) $\rightarrow$ (L + 3)11% (H − 1) $\rightarrow$ (L + 3)11%	463.5[b]	3.18[b]
	316.5[b]	0.33[b]	(H − 4) $\rightarrow$ (L + 3)11%	350.5[b]	1.73[b]
PAF2	426.2	2.93	$S_0 \rightarrow S_1$ (H) $\rightarrow$ (L + 1)28% (H − 1) $\rightarrow$ (L)28%	463.4	3.17
	414.5[b]	3.13[b]	(H − 3) $\rightarrow$ (L)11% (H − 2) $\rightarrow$ (L + 1)11%	482.7[b]	3.19[b]
	315.2	0.27	$S_0 \rightarrow S_{17}$ (H − 1) $\rightarrow$ (L + 11)29% (H) $\rightarrow$ (L + 11)26%	351.4	1.88
	317.9[b]	0.27[b]		356.4[b]	1.97[b]
PE2	387.6	3.59	$S_0 \rightarrow S_1$ (H) $\rightarrow$ (L + 1)37% (H − 1) $\rightarrow$ (L)37%	448.1	3.53
	387.9[b]	3.60[b]		458.7[b]	3.66[b]
	312.5	0.29	$S_0 \rightarrow S_{15}$ (H − 1) $\rightarrow$ (L + 8)10%	358.4	1.23
	313.2[b]	0.29[b]		362.7[b]	1.19[b]
BA2	392.0	2.59	$S_0 \rightarrow S_1$ (H) $\rightarrow$ (L)32% (H − 1) $\rightarrow$ (L + 1)31%	442.3	2.84
	388.2[b]	2.84[b]		456.6[b]	2.88[b]
	384.3	0.45	$S_0 \rightarrow S_4$ (H) $\rightarrow$ (L + 1)33% (H − 1) $\rightarrow$ (L)33%	342.9	1.37
	313.8	0.41	$S_0 \rightarrow S_{20}$ (H − 1) $\rightarrow$ (L + 8)16% (H) $\rightarrow$ (L + 8)14%	345.8[b]	1.47[b]
	314.7[b]	0.28[b]	(H − 1) $\rightarrow$ (L + 6)11%		

H denotes the HOMO and L denotes the LUMO

[a] The experimental data in Hayek et al. [25]

[b] The calculation in methylene chloride

significantly affect the λ_{max}^{O} values but increases the oscillator strengths. On the other hand, replacing a phenyl unit by a pyridine or tetrafluorobenzene unit in the conjugated connectors always leads to significant red-shifts of the UV/Vis absorption (**PAN2**: 6.5 nm and **PAF2**: 36.6 nm vs. **PA2**). Finally, it is noteworthy that the λ_{max}^{O} values of pyrazaboles are bathochromically shifted when increasing either the electron-donating or electron-accepting character of the peripheral groups, indicative of a more pronounced either core-to-periphery or periphery-to-core intramolecular charge transfer [47]. This is confirmed by molecular orbital calculations (see Figure S1). In addition, from Table 1, it can be found that the transition character of all pyrazaboles in the low-energy region is from valence HOMO and HOMO-1 to LUMO and LUMO + 1. Orbital analysis reveals that the π–π^* transitions occur typically at the π-conjugated systems and terminal groups, and the boron atoms of the pyrazabole moiety as a spacer does not participate in these transitions. But in the high-energy region, the electronic transition actually occurs from the terminal moieties to the pyrazabole center (Figure S1). And it has been reported that the intermolecular interaction through π–σ–π likely occurs in the excited state [24, 48, 49]. According to the exciton model theory, purely excitonic coupling should lead to large shifts in both absorption and emission spectra. Thus, taking pyrazabole **PA2** and its "monomer" **A** (see Figure S2) as examples, we perform their ground- and excited-state geometry optimizations by DFT//B3LYP/6-31G* and CIS/6-31G*, respectively. Then on the basis of optimized results, the UV/Vis absorption and fluorescence emission spectra were investigated by TD-DFT//B3LYP/6-31G*. The absorption maxima are located at 436.9 and 415.6 nm for **PA2** and **A**, respectively. That is to say, pyrazabole **PA2** exhibits a slightly large bathochromic shift of 21 nm as compared with the model "monomer" **A**. The fluorescence emission spectra are located at 527.5 and 444.7 nm for **PA2** and **A**, respectively. A significant bathochromic shift of 83 nm is observed for **PA2** in comparison with **A**. These results show a large difference (61.5 nm) in the Stokes shifts of **PA2** and **A**. This indicates that the conjugated systems connected to the pyrazabole core are strongly coupled in the excited state, but weakly coupled in the ground state.

Remarkably, both increasing the conjugated length by the triple or double bond and introducing electron-accepting groups in conjugated connectors lead to marked red-shifts of the maximum absorption. But it can be found that all the constructed pyrazaboles still retain good transparency, which is important for optical power limiting applications.

Since a proper account of the solvent effect is crucial for a direct comparison between experiment and calculations, we perform ZINDO calculations with the inclusion of bulk solvent effects via a PCM as well [47, 50–53]. As can be seen in Table 1, comparing the results in vacuum and using the PCM model in dichloromethane, it is evident that the effect of the solvent shifts slightly except for fluorophores **PA3** and **PAB**. In general, the λ_{max}^{O} of **PA3** in dichloromethane is 35.5 nm larger than that of in vacuum, whereas the λ_{max}^{O} of **PAB** in dichloromethane is 19.6 nm smaller than that of in vacuum. The ΔE_{H-L} of these two molecules are affected obviously by the solvent, which may be attributed to the atoms oxygen and fluorine atoms at the molecular terminals bearing the higher electro-negativity that can lead to larger polarization.

3.4 Two-photon absorption properties

The TPA cross sections of all fluorophores are determined in the 500–1,000 nm region by utilizing the ZINDO-SOS program. Herein, we select the excited states with larger transition dipole moment as the intermediate state, and the position of the maximum TPA (λ_{max}^{T}) is obtained by scanning $\hbar\omega$ in the range of 1.0–4.0 eV. The calculated maximum TPA cross sections (δ_{max}), the TPA maximum wavelength, and transition nature are collected in Table 2. In order to provide a clearer comparison, TPA spectra are presented in Fig. 4. In contrast with the experimental results [25], it is noteworthy that although the calculations with the ZINDO method somehow underestimate δ_{max} values in long-wavelength region, they can nevertheless provide the correct structure-to-property relations for TPA processes, as has been previously reported [53–56]. It should be noticed that the δ_{max} values of pyrazaboles **P1** (702.2 GM at 531.7 nm) and **PAB** (118.1 GM at 710.9 nm) are in good agreement with the experimental data (900 GM at 525 nm, 100 GM at 740 nm), respectively [25]. As shown, all fluorophores exhibit the strongest TPA band at 500–600 nm and the largest δ_{max} values in the range of 540–3,560 GM. This indicates that the pyrazaboles can be used as excellent optical power limiting materials. Moreover, these compounds exhibit somewhat stronger values of δ_{max} in the near-infrared (NIR) spectral region (700–850 nm) except **P1**, **PA1**, **PA4,** and **PAN2**. In particular, the δ_{max} values of **PA3** and **PAF2** are 308.8 GM at 772.0 nm and 157.8 GM at 834.4 nm, respectively. The two constructed fluorophores may be particularly attractive as probes for two-photon fluorescence imaging (TPFM).

While solvent impact on the TPA properties was taken into account by the PCM model, calculations of δ_{max} in methylene chloride are carried out as well (cf. Table 2). In general, the solvent effects on TPA properties are fluxional for different fluorophores with respect to those in gas phase: for instance, **P1** and **PAB** are almost unchanged; for **PA1**, **PA2**, **PA4**, **PAN2,** and **PAF2**, their δ_{max} values of

Table 2 Two-photon absorption properties, λ^T_{max} (nm), δ_{max} (GM)

Mol.	λ^T_{max}	δ_{max}	Channel	Transition nature
P1	581.0 (525[a])	163.9 (900[a])	$S_0 \rightarrow S_1 \rightarrow S_9$	(H − 4) → (L)32% (H − 1) → (L + 4)24%
	581.0[b]	169.7[b]		(H − 1, H − 1) → (L, L)22%
	531.7	702.2	$S_0 \rightarrow S_1 \rightarrow S_{12}$	(H − 3) → (L + 1)44% (H) → (L + 6)23%
	530.3[b]	691.7[b]		(H, H) → (L + 1, L + 1)11%
PA1	566.7 (525[a])	1,419.1 (425[a])	$S_0 \rightarrow S_3 \rightarrow S_{16}$	(H − 3) → (L + 1)17% (H − 2) → (L + 1)16%
	591.0[b]	585.2[b]		(H) → (L + 5)11%
	554.5[b]	1,249.7[b]		
P2	731.0 (800[a])	76.4 (209[a])	$S_0 \rightarrow S_1 \rightarrow S_2$	(H − 1) → (L + 1)36% (H) → (L)22%
	736.3[b]	42.0[b]		(H) → (L + 1)16%
	585.0	833.6	$S_0 \rightarrow S_1 \rightarrow S_{17}$	(H) → (L + 4)15% (H − 2) → (L)14% (H−1) → (L + 4)13%
	563.6	1,170.6	$S_0 \rightarrow S_1 \rightarrow S_{18}$	(H − 3) → (L + 1)16% (H − 1) → (L + 5)13%
	566.7[b]	1,968.5[b]		(H − 2) → (L + 1)11%
PA2	760.6 (800[a])	54.4 (314[a])	$S_0 \rightarrow S_1 \rightarrow S_3$	(H) → (L)43% (H − 1) → (L + 1)24%
	760.4[b]	46.9[b]		
	579.4	2,014.8	$S_0 \rightarrow S_1 \rightarrow S_{24}$	(H − 1) → (L + 5)16% (H − 3) → (L + 1)15%
	577.7[b]	1,878.4[b]		(H − 2) → (L + 1)11%
PA3	772.0	308.8	$S_0 \rightarrow S_5 \rightarrow S_8$	(H − 1) → (L + 1)22% (H) → (L)20%
	851.5[b]	735.5[b]		
	689.6	397.2	$S_0 \rightarrow S_5 \rightarrow S_{11}$	(H) → (L + 11)34% (H − 4) → (L + 2)20%
	725.9[b]	162.7[b]		(H − 1) → (L + 11)17% (H − 4) → (L)11%
	576.1	1,648.6	$S_0 \rightarrow S_5 \rightarrow S_{22}$	(H − 3) → (L + 1)11%
	610.2[b]	2,523.7[b]		
	513.2	1,526.4	$S_0 \rightarrow S_5 \rightarrow S_{25}$	(H) → (L + 6)12%
	518.3[b]	1,627.5[b]		
PA4	591.0	3,560.3	$S_0 \rightarrow S_1 \rightarrow S_{22}$	(H) → (L + 4)19% (H − 1) → (L + 5)12%
	777.8[b]	124.2[b]		(H) → (L + 5)10%
	626.8[b]	2,278.8[b]		
	596.1[b]	1,208.8[b]		
	514.5	854.2	$S_0 \rightarrow S_1 \rightarrow S_{26}$	(H) → (L + 14)11%
PAB	710.9 (740[a])	118.1 (100[a])	$S_0 \rightarrow S_3 \rightarrow S_9$	(H − 2) → (L + 4)26% (H − 3) → (L + 5)26%
	696.5[b]	83.7[b]		
	621.2	100.4	$S_0 \rightarrow S_3 \rightarrow S_{17}$	(H − 4) → (L)32% (H − 5) → (L + 1)32%
	601.2[b]	124.0[b]		(H − 4) → (L + 1)13% (H − 5) → (L)13%
	517.0	539.4	$S_0 \rightarrow S_3 \rightarrow S_{30}$	(H − 10) → (L + 1)57% (H − 10) → (L)35%
PAN2	582.6	2,232.6	$S_0 \rightarrow S_1 \rightarrow S_{25}$	(H − 3) → (L + 1)16%
	694.2[b]	128.8[b]		
	542.8	741.4	$S_0 \rightarrow S_1 \rightarrow S_{28}$	(H) → (L + 16)15% (H − 1) → (L + 17)11%
	576.1[b]	1,650.6[b]		
PAF2	834.4	157.8	$S_0 \rightarrow S_1 \rightarrow S_2$	(H) → (L)30% (H − 1) → (L + 1)30%
	808.2[b]	89.1[b]		(H − 2) → (L)10% (H − 3) → (L + 1)10%
	708.5	486.4	$S_0 \rightarrow S_1 \rightarrow S_8$	(H − 2) → (L)10%
	685.0[b]	524.5[b]		
	594.4	3,087.2	$S_0 \rightarrow S_1 \rightarrow S_{24}$	(H − 2) → (L)14% (H − 3) → (L + 1)14%
	584.3[b]	2,069.4[b]		(H − 3) → (L + 7)11% (H − 2) → (L + 6)10%
	556.0	1,032.3	$S_0 \rightarrow S_1 \rightarrow S_{28}$	(H) → (L + 18)18% (H − 1) → (L + 19)18%
	551.5[b]	978.4[b]		
	515.7	335.9	$S_0 \rightarrow S_1 \rightarrow S_{34}$	(H) → (L + 20)14% (H − 1) → (L + 21)14%

Table 2 continued

Mol.	λ^T_{max}	δ_{max}	Channel	Transition nature
PE2	752.3	79.5	$S_0 \rightarrow S_1 \rightarrow S_2$	(H) → (L)38% (H − 1) → (L + 1)37%
	755.1[b]	55.7[b]		
	597.8	2,184.5	$S_0 \rightarrow S_1 \rightarrow S_{18}$	(H) → (L + 4)14% (H − 2) → (L)12%
	596.1[b]	2,203.1[b]		(H − 3) → (L + 1)11% (H − 1) → (L + 5)11%
	533.0	852.1	$S_0 \rightarrow S_1 \rightarrow S_{22}$	(H − 4) → (L)14% (H − 5) → (L + 1)12%
	534.4[b]	696.4[b]		
BA2	766.3	62.5	$S_0 \rightarrow S_1 \rightarrow S_4$	(H) → (L + 1)33% (H − 1) → (L)33%
	757.9[b]	38.8[b]		
	585.9	2,502.3	$S_0 \rightarrow S_1 \rightarrow S_{24}$	(H − 2) → (L + 1)15% (H − 3) → (L)14%
	585.9[b]	2,532.5[b]		(H − 1) → (L + 4)12%
	541.4	569.6	$S_0 \rightarrow S_1 \rightarrow S_{26}$	(H − 1) → (L + 18) 13% (H) → (L + 19)11%
	540.0[b]	458.8[b]		(H − 1) → (L + 16)11% (H) → (L + 17)11%

H denotes the HOMO and L denotes the LUMO

[a] The experimental data in Hayek et al. [25]

[b] The calculation in methylene chloride

them are reduced, and the strongest peaks of TPA wavelength show blue-shifts except for **PA4**; for **P2**, **PA3**, **PE2**, and **BA2**, the maximum TPA cross sections are increased, the corresponding wavelength values appear quite similar to those in gas phase except **PA3,** and it can also be found that the NIR absorption band exhibits a red-shift. Specially, the solvent has a significant effect on the TPA properties for **PA3**, such as the λ^T_{max} red-shift and δ_{max} intensity increasing. Above analysis indicates the relative changing rules keep almost the same both in gas phase and in methylene chloride. And the TPA properties will be discussed on some structural and other aspects which affect the TPA properties.

3.4.1 Effect of donor or acceptor ability

Regarding Table 2 and Fig. 4a–c, it is worth noting that the maximum TPA cross sections in gas phase enhance with increasing either the electron-donating or electron-withdrawing end-groups, such as **P1** (702.2 GM) < **P2** (1,170.6 GM), **PA1** (1,419.1 GM) < **PA2** (2,014.8 GM), and **PA3** (1,648.6 GM) < **PA4** (3,560.3 GM), following the definite red-shift of the TPA spectra. Thus, fluorophore **PAB** exhibits the largest δ_{max} among push-push chromophores in the NIR absorption band. The solvent has a more significant influence on the TPA properties for pull-pull chromophores as compared to push-push ones, which can be regarded as the consequence of strong π-π interactions. As displayed in Table 2, **PA3** and **PA4** show the largest TPA cross sections separately at 610.2 and 626.8 nm in dichloromethane, whereas the corresponding TPA positions are bathochromatically shifted by nearly 34 and 36 nm from those of the values in gas phase. Interestingly, these two pyrazaboles present new maximum TPA activities of 735.5 GM at 851.5 nm and 124.2 GM at 777.8 nm in dichloromethane in the NIR region. The predicted results can confirm that the constructed pull-pull chromophores may be used for two-photon excited microscopy bioimaging according to the experimental result of bis-BODIPY derivative **PAB** [25].

3.4.2 Effect of π-bridging

Replacing a phenyl unit by a pyridine or tetrafluorobenzene unit in the conjugated connectors always leads to a significant red-shift of the TPA spectrum, that is, **PA2** (579.4 nm) < **PAN2** (582.6 nm) < **PAF2** (594.4 nm) (Table 2; Fig. 4d). Also a distinct increase in the TPA efficiency is observed. For instance, **PAF2** displays a maximum TPA cross section that is 1.5 times as large as that of **PA2** at about 600 nm and ninefold greater than that in the NIR region. Especially, it exhibits δ_{max} of 157.8 GM at 834.4 nm, which is important for TPEM applications.

As one can notice from Table 2, fluorophore **PE2** containing the ethylene moiety exhibits larger δ_{max} (by 1.1 times) than **PA2** with acetylene π-bridged counterpart. Recently, Bhaskar [57] and Zahradník et al. [23] have explained the higher TPA cross sections of alkene chromophores compared to their alkyne counterparts by using time-resolved measurements. These measurements have revealed a greater amount of charge transfer in alkene π-bridged systems by virtue of a greater population of the conformationally and solvent-related ICT state. In contrast, the TPA efficiency of the triple-bond analog **PA2** does not differ too much from that of **PE2**, and since the quantum yield, the molecular planarity, steric congestion, and other

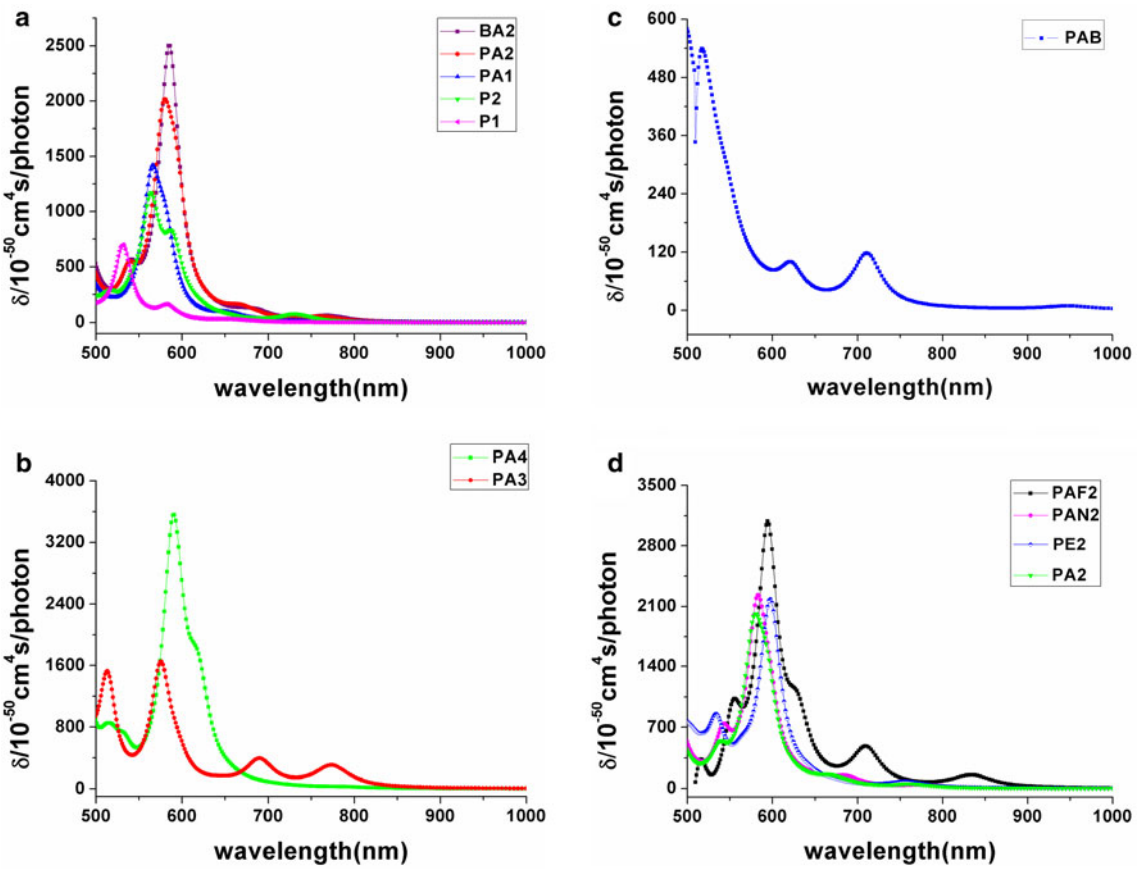

Fig. 4 Two-photon absorption spectra for all the molecules

respects are considered, acetylene-linked systems could sometimes be viewed as a suitable candidate for practical applications as well.

3.4.3 *Effect of length*

Increasing the conjugated length induces a significant enhancement of δ_{max}. Namely, the value of **PA1** (1,419.1 GM) or **PA2** (2,014.8 GM) is twofold greater than that of **P1** (702.2 GM) or **P2** (1,170.6 GM), respectively (Fig. 4a). Moreover, we observe a marked red-shift and definite broadening of the TPA spectrum. Similar changes in TPA activity have also been reported theoretically for other molecular structures [8, 47, 58, 59]. This result can be ascribed to the ethynylene-linker extending the conjugated length and steadying the molecular planarity.

3.4.4 *Effect of central core*

To assess the influence of central moiety on the TPA properties, we compare δ_{max} of **PA2** with that of its analog **BA2**, where the methyl groups at the boron atoms are all replaced by fluorine. From Table 2 and Fig. 4a, it is obvious that fluorophore **BA2** is somehow superior to **PA2**. Specifically, the δ_{max} of **BA2** increases by 487.5 GM and λ_{max}^{T} show bathochromic shift by 6.5 nm as compared to **PA2**. It is contributed to stronger ICT ability when the electron acceptors are incorporated into the boron atoms.

Generally, the position and relative strength of the two-photon resonance could be predicted with the following three-level energy model simplified form of the SOS expression [18, 44, 60]:

$$\delta \propto \frac{M_{0k}^2 M_{kn}^2}{(E_{0k} - E_{0n}/2)^2 \Gamma} + \frac{M_{0n}^2 \Delta\mu_{0n}^2}{(E_{0n}/2)^2 \Gamma} \quad (4)$$

Here, M_{ij} is the transition dipole moment from the state i to j; E_i is the corresponding excitation energy, the subscripts 0, k, and n refer to the ground state S_0, the intermediate state S_k, and the TPA final state S_n, respectively; $\Delta\mu_{0n}$ is the state dipole moment difference between S_0 and S_n; the damping factor Γ is set to 0.1 eV.

Table 3 lists some important linear absorption parameters for the intermediate and final states of two-photon absorption of studied compounds. According to the results in Table 3, the relationship between the maximum TPA cross section δ_{max} and $M_{0k}^2 M_{kn}^2/[(E_{0k} - E_{0n}/2)^2\Gamma] +$

Table 3 Linear optical parameters of two-photon absorption for fluorophores, $X = \frac{M_{0k}^2 M_{kn}^2}{(E_{0k}-E_{0n}/2)^2\Gamma} + \frac{M_{0n}^2 \Delta\mu_{0n}^2}{(E_{0n}/2)^2\Gamma}$, E_{0k}, E_{kn}(eV)

Mol.	Channels	M_{0k}	M_{kn}	M_{0n}	E_{0k}	E_{0n}	E_{0k}–$E_{0n}/2$	$\Delta\mu_{0n}$	X	δ_{max}
P1	$S_0 \rightarrow S_1 \rightarrow S_9$	12.40	3.83	1.31	3.64	4.26	1.51	0.18	9,899.03	163.9
	$S_0 \rightarrow S_1 \rightarrow S_{12}$		7.44	1.25		4.67	1.31	0.00	49,961.25	702.2
PA1	$S_0 \rightarrow S_3 \rightarrow S_{16}$	13.43	6.96	0.74	3.26	4.39	1.07	0.08	76,966.87	1,419.1
P2	$S_0 \rightarrow S_1 \rightarrow S_2$	14.76	5.14	4.49	3.32	3.39	1.63	1.43	21,946.45	76.4
	$S_0 \rightarrow S_1 \rightarrow S_{17}$		8.84	1.78		4.21	1.22	2.13	115,369.84	833.6
	$S_0 \rightarrow S_1 \rightarrow S_{18}$		6.98	1.39		4.40	1.12	1.73	84,602.11	1,170.6
PA2	$S_0 \rightarrow S_1 \rightarrow S_3$	15.69	3.04	4.61	3.18	3.25	1.56	1.09	9,491.15	54.4
	$S_0 \rightarrow S_1 \rightarrow S_{24}$		9.11	1.04		4.29	1.04	1.41	190,855.26	2,014.8
PA3	$S_0 \rightarrow S_5 \rightarrow S_8$	14.28	8.14	3.69	3.14	3.20	1.54	2.15	57,162.24	308.8
	$S_0 \rightarrow S_5 \rightarrow S_{11}$		0.41	0.38		3.71	1.29	0.24	197.46	397.2
	$S_0 \rightarrow S_5 \rightarrow S_{22}$		8.44	0.95		4.31	0.99	2.92	149,539.38	1,648.6
	$S_0 \rightarrow S_5 \rightarrow S_{25}$		4.06	1.35		4.81	0.74	3.85	62,098.20	1,526.4
PA4	$S_0 \rightarrow S_1 \rightarrow S_{22}$	17.87	8.73	1.08	3.09	4.21	0.99	2.68	251,044.66	3,560.3
	$S_0 \rightarrow S_1 \rightarrow S_{26}$		1.87	1.09		4.77	0.71	0.11	22,425.49	854.2
PAB	$S_0 \rightarrow S_3 \rightarrow S_9$	10.19	0.38	1.85	2.61	3.59	0.82	0.16	229.68	118.1
	$S_0 \rightarrow S_3 \rightarrow S_{17}$		0.90	0.79		3.99	0.62	0.61	2,360.26	100.4
	$S_0 \rightarrow S_3 \rightarrow S_{30}$		0.43	0.04		4.86	0.18	16.14	6,047.51	539.4
PAN2	$S_0 \rightarrow S_1 \rightarrow S_{25}$	15.57	8.51	1.63	3.13	4.26	1.00	0.10	175,660.31	2,232.6
	$S_0 \rightarrow S_1 \rightarrow S_{28}$		2.44	0.88		4.58	0.84	0.00	20,499.88	741.4
PAF2	$S_0 \rightarrow S_1 \rightarrow S_2$	16.30	6.35	3.52	2.91	2.97	1.43	1.41	52,895.58	157.8
	$S_0 \rightarrow S_1 \rightarrow S_8$		6.48	0.24		3.49	1.17	0.43	82,221.12	486.4
	$S_0 \rightarrow S_1 \rightarrow S_{24}$		9.58	1.06		4.17	0.83	0.20	358,151.36	3,087.2
	$S_0 \rightarrow S_1 \rightarrow S_{28}$		3.22	0.32		4.48	0.67	1.13	61,171.88	1,032.3
	$S_0 \rightarrow S_1 \rightarrow S_{34}$		2.76	0.76		4.82	0.50	1.60	81,160.70	335.9
PE2	$S_0 \rightarrow S_1 \rightarrow S_2$	17.19	4.39	4.04	3.20	3.28	1.56	1.05	23,486.25	79.5
	$S_0 \rightarrow S_1 \rightarrow S_{18}$		11.14	0.46		4.15	1.08	0.50	317,449.26	2,184.5
	$S_0 \rightarrow S_5 \rightarrow S_{22}$		3.63	0.14		4.64	0.88	0.46	50,388.08	852.1
BA2	$S_0 \rightarrow S_1 \rightarrow S_4$	14.68	3.38	6.05	3.16	3.23	1.55	1.43	10,628.09	62.5
	$S_0 \rightarrow S_1 \rightarrow S_{24}$		9.96	1.01		4.24	1.04	0.76	197,561.56	2,502.3
	$S_0 \rightarrow S_1 \rightarrow S_{26}$		1.84	0.85		4.59	0.87	0.41	9,768.48	569.6

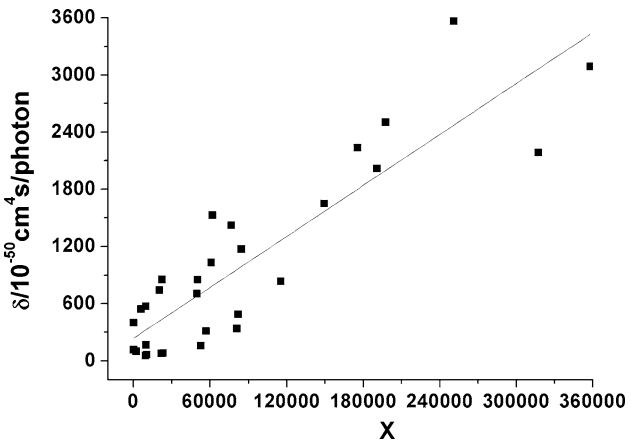

Fig. 5 Plot of δ_{max} versus $X(M_{0k}^2 M_{kn}^2/[(E_{0k} - E_{0n}/2)^2\Gamma] + \Delta\mu_{0n}^2 M_{0n}^2/[(E_{0n}/2)^2\Gamma])$

$\Delta\mu_{0n}^2 M_{0n}^2/[(E_{0n}/2)^2\Gamma]$ is depicted in Fig. 5. As can be seen, the calculated points are averagely distributed on the two sides of the line. The relationship of them is directly proportional in accordance with Eq. 4. As shown in Table 3 and Fig. 5, we can draw conclusions as followed: (1) Increasing the conjugated length leads to enhancement of the transition dipole moment (M_{0k}) between the ground state and intermediate state and reduction of the energy tuning term (E_{0k}–$E_{0n}/2$). (2) The replacement of a triple bond by a double bond in conjugated linker results in the increase of M_{0k} and M_{kn} (the transition dipole moment between the intermediate state and final state). The increase of the transition dipole moments is the main reason that alkene π-conjugated chromophores have somewhat superior TPA properties over their alkyne π-conjugated analogs. (3) Replacing a phenyl unit by a pyridine or

tetrafluorobenzene unit in the conjugated connectors always leads to increased M_{kn} and reduced $(E_{0k}-E_{0n}/2)$. Therefore, the enhancement of $\delta_{\max}$ is in the order **PA2** < **PAN2** < **PAF2**. (4) When the strength of electron-donating or electron-accepting terminal groups increases, both M_{0k} and M_{kn} enhance, while $(E_{0k}-E_{0n}/2)$ reduce or remain unchanged. (5) Substitution of the methyl at the boron atoms with fluorine produces M_{kn} increasing, which is the main reason why **BA2** possesses the larger TPA cross section than that of **PA2**. (6) According to the above conclusion and analysis for Table 3, the latter part of the three-state model is small and can be ignored compared to the former part. In a word, the excitation energy (E_{0k}, E_{0n}) and the transition dipole moment (M_{0k}, M_{kn}) are two important parameters for two-photon absorption cross section of the pyrazabole chromophores.

In order to gain insight into the effect of the pyrazabole core on two-photon absorption properties and further confirm the role of intramolecular interactions, we list the frontier molecular orbitals related to main transitions in the two-photon absorption. First, it can be seen from Table 2 that the more inner molecular orbitals such as HOMO-5, HOMO-4, HOMO-3, and LUMO + 4, LUMO + 5, LUMO + 7 contribute to the TPA transitions. As shown in Figure S1 (in the Supporting Information), there are some contributions from the pyrazabole moiety in these higher energy molecular orbitals. It should be concluded that the incorporation of pyrazabole moiety results in effective coupling interaction and thus leads to the enhancement of TPA cross sections. Second, for pyrazabole fluorophores with electron-donating end-groups, the electron clouds of HOMO are contributed by the electron-donating and π-conjugated segments, while the electron clouds of LUMO are delocalized on the center or the whole molecule. It is obviously found that the electron transfer occurs between the donor group and the center or the whole molecule during the TPA process. So the higher electron transfer the molecule has, the larger TPA cross sections the molecule exhibits, such as molecule **PA2** (2,014.8 GM) > **PA1** (1,419.1 GM). In contrast, for the fluorophores with electron-accepting groups, the intramolecular electron transfer is observed from the whole molecule or the center to the acceptor moiety.

Since aluminum has the same number of valence electrons as boron, it is quite natural to wonder that organoaluminum dyes could behave similarly to organoborons in optical properties. However, to the best of our knowledge, in contrast to the pyrazaboles, the compounds with the Al_2N_4 central core remain largely unknown. To predict the OPA and TPA properties of organoaluminum dyes, we take the molecule **AlA2** (substitution of the boron atoms of pyrazabole **PA2** by aluminum) as example in this paper. To ensure the direct comparison, we also perform calculations on **AlA2** at the same methods. The optimized ground-state geometry of molecule **AlA2** (see Figure S3) and some important parameters (Table S3) are all shown in the Supporting Information. As shown in Fig. 2 and Figure S3, molecule **AlA2** has the similar structure to **PA2** but exhibits a more obvious bent shape and with the lower energy. From Table S3, it can be observed that the bonds Al(1)–N(3) and N(3)–N(4) of molecule **AlA2** are distinctly larger than the bonds B(1)–N(3) and N(3)–N(4) of **PA2**, whereas other bonds are quite similar. The angles N(5)–Al(1)–N(3) and Al(1)–N(3)–N(6)–Al(2) of molecule **AlA2** are small, but Al(1)–N(3)–N(4) and C(15)–Al(1)–C(16) are large with respect to **PA2**. This implies that the central ring Al_2N_4 is larger than B_2N_4 in the molecular size and has a large dipole moment [3.3643 D (**AlA2**) > 2.2088 D (**PA2**)], which may affected the linear optical and TPA properties. As shown in Table S4, the UV/Vis absorption of molecule **AlA2** is located at 385.2 nm and slightly blue-shifted by 4.4 nm as compared to **PA2**. The maximum TPA cross section of molecule **AlA2** increases by 301.5 GM relative to **PA2** and is almost located at the same TPA wavelength. From the calculations of molecule **AlA2**, we can draw the conclusion that the compounds with Al_2N_4 center behave similarly to pyrazaboles in the linear optical and TPA properties and increase TPA cross sections to some extent.

4 Conclusions

The systematic investigation of the geometric and electronic structures as well as linear and nonlinear optical properties on such a novel series of pyrazabole chromophores is of great importance for both tuning electronic spectra and designing TPA materials. The influence of each moiety constituting the structures (cores, π-conjugated bridges, and end-groups), and solvent on OPA and TPA properties was theoretically studied in detail. All the target pyrazaboles exhibit an intense absorption in the near UV/Vis blue region. Substitution of the methyl groups at the boron atoms with fluorine atoms, replacing a phenyl unit by a pyridine or tetrafluorobenzene unit in the conjugated connectors, increasing the conjugated length, and the end-groups strength induces a significant bathochromic shift of the absorption band, which is just corresponding to the ΔE_{H-L} above. The solvent results indicate that they slightly affect OPA property slightly except for fluorophores **PA3** and **PAB** and appear fluxional for different pyrazabole fluorophores relative to those in gas phase. And then these factors further influence TPA cross sections. In general, by incorporating electron acceptors in the central core, π-conjugated bridge, or terminal groups, the TPA cross sections increase. The solvent has a significant effect on the

TPA properties for **PA3** and leads to the λ^{T}_{max} red-shift and δ_{max} intense increasing. All pyrazabole derivatives exhibit the strongest TPA band at 500–600 nm and the largest δ_{max} values in the range of 540–3,560 GM, indicating they may be potential TPA materials for the application of optical power limiting. It is noteworthy that the δ_{max} values of **PA3** and **PAF2** are 308.8 GM at 772.0 nm and 157.8 GM at 834.4 nm, respectively. The two constructed fluorophores may be particularly attractive as probes for two-photon fluorescence imaging. Furthermore, from the calculations of molecule **AlA2**, we can draw the conclusion that the compounds with the Al_2N_4 center behave similarly to pyrazabole chromophores in the linear optical and TPA properties and increase TPA cross sections to some extent.

Acknowledgments This work is supported by the Natural Science Foundation of China (No. 20973078 and 20673045), Special Funding to Basic Scientific Research Projects for Central Collages as well as the Open Project of the State Key Laboratory for Supramolecular Structure and Material of Jilin University (SKLSSM200716). The reviewers' invaluable suggestions and comments are greatly appreciated.

References

1. Zipfel WR, Williams RM, Webb WW (2003) Nat Biotechnol 21: 1369–1377
2. Xing J-F, Dong X-Z, Chen W-Q, Duan X-M, Takeyasu N, Tanaka T, Kawata S (2007) Appl Phys Lett 90:131106 (1–3)
3. Kawata S, Kawata Y (2000) Chem Rev 100:1777–1788
4. Bouit PA, Wetzel G, Berginc G, Loiseaux B, Toupet L, Feneyrou P, Bretonnière Y, Kamada K, Maury O, Andraud C (2007) Chem Mater 19:5325–5335
5. Belfield KD, Corredor CC, Morales AR, Dessources MA, Hernandez FE (2006) J Fluoresc 16:105–110
6. Lin TC, Chung SJ, Kim KS, Wang X, He GS, Swiatkiewicz J, Pudavar HE, Prasad PN (2003) Adv Polym Sci 161:157–193
7. Opanasyuk O, Ryderfors L, Mukhtar E, Johansson LB-Å (2009) Phys Chem Chem Phys 11:7152–7160
8. Pawlicki M, Collins HA, Denning RG, Anderson HL (2009) Angew Chem Int Ed 48:3244–3266
9. Kim HM, Cho BR (2009) Chem Commun 153–164
10. Kim HM, Seo MS, Jeon SJ, Cho BR (2009) Chem Commun 7422–7424
11. Kamada K, Iwase Y, Sakai K, Kondo K, Ohta K (2009) J Phys Chem C 113:11469–11474
12. Fitilis I, Fakis M, Polyzos I, Giannetas V, Persephonis P, Vellis P, Mikroyannidis J (2007) Chem Phys Lett 447:300–304
13. Chakrabarti S, Ruud K (2009) Phys Chem Chem Phys 11: 2592–2596
14. Zein S, Delbecq F, Simon D (2009) Phys Chem Chem Phys 11: 694–702
15. Nguyen KA, Day PN, Pachter R (2008) Theor Chem Acc 120: 167–175
16. Wang CK, Macak P, Luo Y, Agren H (2001) J Chem Phys 114:9813–9820
17. Rudberg E, Salek P, Helgaker T, Agren H (2005) J Chem Phys 123:184108-1–184108-7
18. Rumi M, Ehrlich JE, Heikal AA, Perry JW, Barlow S, Hu Z-Y, McCord-Maughon D, Parker TC, Röckel H, Thayumanavan S, Marder SR, Beljonne D, Brédas J-L (2000) J Am Chem Soc 122:9500–9510
19. Shao P, Huang B, Chen LQ, Liu ZJ, Qin JG, Gong HM, Ding S, Wang QQ (2005) J Mater Chem 15:4502–4506
20. Abbotto A, Beverina L, Bozio R, Facchetti A, Ferrante C, Pagani GA, Pedron D, Signorini R (2002) Org Lett 4:1495–1498
21. Zheng SJ, Beverina L, Barlow S, Zojer E, Fu J, Padilha LA, Fink C, Kwon O, Yi YP, Shuai ZG, Van Stryland EW, Hagan DJ, Bredas JL, Marder SR (2007) Chem Commun 1372–1374
22. Zou L, Liu ZJ, Yan XB, Liu Y, Fu Y, Liu J, Huang ZL, Chen XG, Qin JG (2009) Eur J Org Chem 32:5587–5593
23. Hrobáriková V, Hrobárik P, Gajdoš P, Fitilis I, Fakis M, Persephonis P, Zahradník P (2010) J Org Chem 75:3053–3068
24. Hayek A, Nicoud J-F, Bolze F, Bourgogne C, Baldeck PL (2006) Angew Chem Int Ed 45:6466–6469
25. Hayek A, Bolze F, Bourgogne C, Baldeck PL, Didier P, Arntz Y, Mély Y, Nicoud J-F (2009) Inorg Chem 48:9112–9119
26. Chow YL, Johansson CI, Zhang Y-H, Gautron R, Yang L, Rassat A, Yang S-Z (1996) J Phys Org Chem 9:7–16
27. Matsumoto F, Chujo Y (2003) Macromolecules 36:5516–5519
28. Cavero E, Lydon DP, Uriel S, de la Fuente MR, Serrano J-L, Gimenez R (2007) Angew Chem Int Ed 46:5175–5177
29. Barbera J, Gimenez R, Serrano JL (2000) Chem Mater 12: 481–489
30. Barberá J, Giménez R, Serrano JL (1994) Adv Mater 6:470–476
31. Matsumoto F, Nagata Y, Chujo Y (2005) Polym Bull 53:155–160
32. Matsumi N, Chujo Y (2008) Polym J 40:77–89
33. Cavero E, Giménez R, Uriel S, Beltrán E, Serrano JL, Alkorta I, Elguero J (2008) Cryst Growth Des 8:838–847
34. Frisch MJ, Trucks GW, Schlegel HB, Scuseria GE, Robb MA, Cheeseman JR, Montgomery JA Jr, Vreven T, Kudin KN, Burant JC, Millam JM, Iyengar SS, Tomasi J, Barone V, Mennucci B, Cossi M, Scalmani G, Rega N, Petersson GA, Nakatsuji H, Hada M, Ehara M, Toyota K, Fukuda R, Hasegawa J, Ishida M, Nakajima T, Honda Y, Kitao O, Nakai H, Klene M, Li X, Knox JE, Hratchian HP, Cross JB, Bakken V, Adamo C, Jaramillo J, Gomperts R, Stratmann RE, Yazyev O, Austin AJ, Cammi R, Pomelli C, Ochterski JW, Ayala PY, Morokuma K, Voth GA, Salvador P, Dannenberg JJ, Zakrzewski VG, Dapprich S, Daniels AD, Strain MC, Farkas O, Malick DK, Rabuck AD, Raghavachari K, Foresman JB, Ortiz JV, Cui Q, Baboul AG, Clifford S, Cioslowski J, Stefanov BB, Liu G, Liashenko A, Piskorz P, Komaromi I, Martin RL, Fox DJ, Keith T, Al-Laham MA, Peng CY, Nanayakkara A, Challacombe M, Gill PMW, Johnson B, Chen W, Wong MW, Gonzalez C, Pople JA (2004) Gaussian 03, Revision C.02. Gaussian, Wallingford
35. Frisch MJ et al (2010) Gaussian 09, Revision B.01. Gaussian, Wallingford
36. Tomasi J, Persico M (1994) Chem Rev 94:2027–2094
37. Cammi R, Cossi M, Tomasi J (1996) J Chem Phys 104: 4611–4620
38. Cammi R, Cossi M, Mennucci B, Tomasi J (1996) J Chem Phys 105:10556–10564
39. Cha M, Torruellas WE, Stegeman GI, Horsthuis WHG, Möhlmann GR, Meth J (1994) Appl Phys Lett 65:2648–2650
40. Kogej T, Beljonne D, Meyers F, Perry JW, Marder SR, Brédas JL (1998) Chem Phys Lett 298:1–3
41. Orr BJ, Ward JF (1971) Mol Phys 20:513–526
42. Bishop DM, Luis JM, Kirtman B (2002) J Chem Phys 116:9379–9729
43. Beljonne D, Wenseleers W, Zojer E, Shuai Z, Vogel H, Pond SJK, Perry JW, Marder SR, Brédas JL (2002) Adv Funct Mater 12:631–641

44. Albota M, Beljonne D, Brédas JL, Ehrlich JE, Fu JY, Heikal AA, Hess SE, Kogej T, Levin MD, Marder SR, McCord-Maughor D, Perry JW, Röckel H, Rumi M, Subramaniam G, Webb WW, Wu XL, Xu C (1998) Science 281:1653–1656
45. Niedenzu K, Nöth H (1983) Chem Ber 116:1132–1135
46. Hanecker E, Hodgkins TG, Niedenzu K, Nöth H (1985) Inorg Chem 24:459–462
47. Mongin O, Porrès L, Charlot M, Katan C, Blanchard-Desce M (2007) Chem Eur J 13:1481–1498
48. Gaab KM, Thompson AL, Xu J, Martinez TJ, Barbeen CJ (2003) J Am Chem Soc 125:9288–9289
49. Thompson AL, Gaab KM, Xu J, Martinez TJ, Barbeen CJ (2004) J Phys Chem A 108:671–682
50. Luo Y, Norman P, Macak P, Agren H (2000) J Phys Chem A 104:4718–4722
51. Nguyen KA, Day PN, Pachter R (2007) J Chem Phys 126:094303-1–094303-10
52. Frediani L, Rinkevicius Z, Agren H (2005) J Chem Phys 122:244104-1–244104-12
53. Zhao Y, Ren A-M, Feng J-K, Zhou X, Ai X-C, Su W-J (2009) Phys Chem Chem Phys 11:11538–11545
54. Zhou X, Ren AM, Feng JK (2004) Chem Eur J 10:5623–5631
55. Yang ZD, Feng JK, Ren AM, Sun CC (2008) Inorg Chem 47:10841–10850
56. Liu XT, Zhao Y, Ren AM, Feng JK J Mol Model. doi: 10.1007/s00894-010-0839-9
57. Bhaskar A, Ramakrishna G, Lu ZK, Twieg R, Hales JM, Hagan DJ, Van Stryland E, Goodson T (2006) J Am Chem Soc 128:11840–11849
58. Padilha LA, Webster S, Przhonska OV, Hu H, Peceli D, Ensley TR, Bondar MV, Gerasov AO, Kovtun YP, Shandura MP, Kachkovski AD, Hagan DJ, Van Stryland EW (2010) J Phys Chem A 114:6493–6501
59. Padilha LA et al (2009) J Mater Chem 19:7503–7513
60. Beljonne D, Wenseleers W, Zojer E, Shuai Z, Vogel H, Pond SJK, Perry JW, Marder SR, Brédas JL (2002) Adv Funct Mater 12:631–641